

# Comet deflection by directed energy: a finite element analysis

Jonathan Madajian<sup>1 a\*</sup>, Janelle Griswold<sup>2 a\*</sup>, Anush Gandra<sup>a</sup>, Gary B. Hughes<sup>b</sup>,  
Qicheng Zhang<sup>a</sup>, Nic Rupert<sup>a</sup>, and Philip Lubin<sup>3a</sup>

<sup>a</sup>Physics Department, University of California, Santa Barbara, CA 93106-9530

<sup>b</sup>Statistics Department, California Polytechnic State University, San Luis Obispo, CA 93407-0405

## ABSTRACT

Comets and asteroids pose a significant threat to our planet. Although the majority of space rocks smaller than 25 meters disintegrate during their decent through Earth's atmosphere, larger objects have the potential to penetrate this protective layer and cause extensive damage. A mile-wide asteroid travelling at 30,000 miles per hour has an impact energy equivalent to a large megaton (Mt) bomb and would likely wipe out most of the life on Earth. Residents near Chelyabinsk, Russia experienced the detrimental effects of a collision with a Near-Earth Asteroid (NEA) on February 15, 2013 when an ~20 m object penetrated the atmosphere above the city. The effective yield from the object's impact was equivalent to a ~1/2 Mt TNT explosion, comparable to that of a large strategic warhead. Previously, in 1908, Russia had experienced an impact thirty times larger, the Tunguska event, which had the estimated yield equivalent to an ~15 Mt TNT explosion. Thankfully, both of these events occurred in relatively remote areas of the globe; however, it would have only taken a minuscule fluctuation in trajectory to redirect these objects to a heavily populated area, resulting in extensive damages and death. In the face of such danger, a planetary defense system is a necessity. The proposed DE-STAR (Directed Energy System for Targeting of Asteroids and exploRation) is a phased array laser system that is capable of, but not limited, ablation, deflection, and de-spinning both asteroids and comets. This paper is a continuation of previous papers that detail the design and applications of such a system, including remote composition analysis, asteroid mining, and interstellar travel. The thrust induced by various DE-STAR configurations on numerous comets is simulated through finite element analysis (FEA), adhering and adjusting to their unique physical properties, such as their rotation rates, emissivity, thermal conductivity, etc.

**Keywords:** DE-STAR, Directed Energy, Laser, Phased Array, Planetary Defense, Comet

## 1. INTRODUCTION

The Directed Energy System for Targeting of Asteroids and exploRation, **DE-STAR**, is a modular phased array of lasers that will be used to destroy or deflect an incoming asteroid or comet.<sup>1</sup> When target fluxes are high enough to vaporize all known constituent materials found on comets and asteroids, (ranging from  $10^4$ - $10^7$  W m<sup>-2</sup> depending on the material being ablated), vaporization will begin and, consequently, mass ejection will take place. This mass ejection will create a reaction force large enough to cause the comet to change its trajectory. If the comet is small enough, the same laser can be used to ablate it entirely. Alternatively, larger comets can be de-spun or deflected. A final option is to spin them up past their gravitational limit to induce structural collapse. While DE-STAR can be used to deflect most incoming bodies, this paper presents a method for simulating the resultant thrust vector on comets from a hypothetical DE-STAR system using a 4D numeric solver, Comsol.

---

<sup>1</sup> Coauthor\*: [JMadajian@gmail.com](mailto:JMadajian@gmail.com)

<sup>2</sup> Coauthor\*: [GriswJa@gmail.com](mailto:GriswJa@gmail.com)

<sup>3</sup> Primary Investigator: [Lubin@deepspace.ucsb.edu](mailto:Lubin@deepspace.ucsb.edu)

\* These authors contributed equally to this work.

Group Website: [www.deepspace.ucsb.edu/](http://www.deepspace.ucsb.edu/)

Comsol Website: [www.comsol.com/](http://www.comsol.com/)

## 2. DE-STAR

DE-STAR is a large standoff laser phased array classified by the common log of its linear size. For example, DE-STAR 0 is 1 m, while a DE-STAR 4 is 10 km.<sup>1,2,4</sup> A large array is necessary to provide full standoff protection, resulting in a baseline system of either a DE-STAR 3 or 4 (1-10 km array) necessary. While small, asteroids and comets can be diverted or vaporized with a DE-STAR 2, 100 m in length; whereas, DE-STAR 0 (1 m array) and DE-STAR 1 (10 m array), can vaporize space debris. Each system, regardless of size, consists of an array of phase-locked, kW class, laser power amplifiers that are driven by a common seed laser. Because the system can be phase-locked, energy can be delivered more efficiently to distant targets. The array of phase-locked modest-power laser amplifiers is powered by solar photovoltaics, of essentially the same area as the laser array. By increasing the array size, it is possible to reduce the spot size due to diffraction and increase the power. Given a gigantic laser array, this dual effect allows the vaporization of elements and compounds on the surface of stellar bodies at solar-scale distances. For example, with a DE-STAR 4, vaporization can occur at over 1 AU. The flux  $W m^{-2}$  on a target scales by  $d^4$ , where  $d$  is the linear dimension of the laser array.<sup>1</sup>

The phased array configuration is capable of creating multiple beams, resulting in a single DE-STAR of sufficient size having the ability to simultaneously vaporize and deflect multiple objects or an object that has broken apart.<sup>1</sup> DE-STAR is intrinsically a multi-tasking system, the phased array configuration consists of a large number of elements that can be simultaneously used for multiple purposes and a wide variety of other functions. DE-STAR may allow standoff analysis through the observation of absorption lines in the blackbody spectrum of a vaporizing surface spot.<sup>1</sup> As discussed, in detail, in Riley et al. (2014), wide-field surveys using narrow bandwidth and precision beam control would aid with asteroid and comet identification and ephemeris refinement. The narrow bandwidth allows for extremely low background searches as well as Doppler velocity determination.<sup>3</sup> While DE-STAR remains a long term vision, a much smaller system, DE-STARLITE, is capable of being launched on a single SLS Block 1B or smaller launcher. DE-STARLITE serves much the same function but requires long lead times and a dedicated mission for each target.<sup>4</sup> This is covered in detail in Kosmo et al. (2014). The same critical issue of rotation is relevant to both. The work presented here is applicable to both a DE-STAR and DE-STARLITE systems.

## 3. COMETS

### 3.1. The Yarkovsky-O'Keefe-Radzievskii-Paddack (YORP) Effect

Infrared radiation escaping from bodies that are heated by the sun carries momentum and heat. Each escaping photon has a momentum, given by  $E/c$ , where  $E$  is the energy of the photon and  $c$  is the speed of light. Re-emission of photons from the surface of an object causes a change in the object's spin rate, due to the photons carrying away momentum and exerting a force on the object. This overall propulsion causes a net torque, affecting the period of rotation and axis of rotation. Although the effect of these photons over a small interval of time is negligible, the net torque over time becomes significant, since numerous objects spend eons in orbit and can be discovered years before potentially colliding with Earth. Objects that rotate in the same direction as their orbit are called prograde rotators, and are driven in the same direction as their orbit and therefore the YORP effect increases their rate of rotation. Retrograde rotators on the other hand undergo the opposite effect, rotating more slowly as time progresses.<sup>5</sup> The asteroid 1862 Apollo has a diameter of 1.5 km and has been observed to increase in one additional orbit rotation cycle over the last 40 years, resulting in a decrease in its orbital rotation period that is clearly visible in photometric lightcurves.<sup>10</sup> Due to the changes of spin rates and orbit rotation period, some speculate that the YORP effect causes structural alterations on the surface, due to mass shedding, thus reducing angular momentum. Many factors must be taken into consideration such as size, shape, spin, mass in the process of predicting changes in momentum.<sup>6</sup>

Another factor that influences the YORP effect is the thermal conductivity of compounds on the object's surface. If the spin rate and shape are known, the YORP effect could be used to model accurate trajectories. Through observation of the strength of the YORP effect, it is also possible to estimate the mass of small objects; additionally, given that the shape and size are known sufficiently well, density could also be inferred. What this means for our project is that after correcting for the YORP effect it might be beneficial to rotate prograde rotators past their gravitational limit and de-spin retrograde rotators so that they can be deflected. The YORP effect can be used to our advantage to increase the effectiveness of DE-STAR.<sup>6</sup>

### 3.2. Properties of Ice

	A [mmHg]	B [mmHg]	C [mmHg]
< 273.15°C	10.5260929208877	2713.06932614349	275.037692824559
> 273.15°C	8.05573	1723.64	233.076

**Table 1. H<sub>2</sub>O<sub>(s)</sub> Antoine coefficients<sup>8,9</sup>** These are the two sets of Antoine coefficients that were used while calculating the temperature and the thrust of the comet while under the directed energy beam.

Since H<sub>2</sub>O<sub>(s)</sub> is the commonly considered to comprise the bulk of comet surface composition, a uniform distribution of H<sub>2</sub>O<sub>(s)</sub> was assumed in our models. Because of water's intrinsic thermal properties, two sets of Antoine coefficients were used when running simulations and are in Table 1. These were determined prior, based on theoretical calculations of the flux. These values were used to determine the vapor pressure within the COMSOL model.

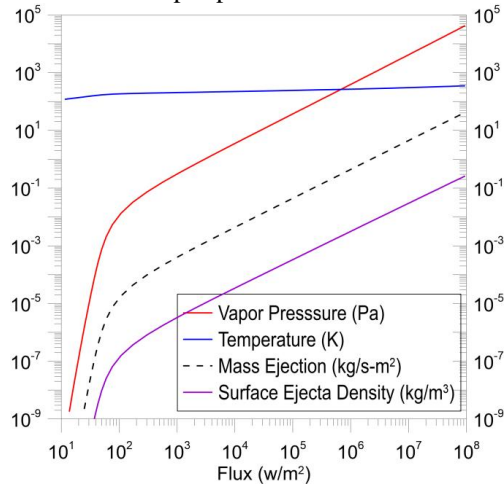


**Figure 1. H<sub>2</sub>O<sub>(s)</sub> Various Parameters vs Flux.** This graph was calculated from analytical values to determine the range of fluxes that would produce the maximum thrust. As you can see the temperature does not vary greatly, but the vapor pressure increases exponentially, starting at a small flux, up to ~100 W m<sup>-2</sup>, and then transitioning to a linear regime.

Figure 1 shows various parameters of H<sub>2</sub>O<sub>(s)</sub> versus flux that were obtained analytically. At low fluxes, the vapor pressure increases exponentially, until approximately a flux of 100 kW m<sup>-2</sup> is obtained; then, the vapor pressure increases linearly. The change in temperature is not dramatic, but does correlate with the vapor pressure. The amount of power from the laser required to reach desired flux levels can, of course, fluctuate, depending on the size of the comet and  $\sigma$  used in the simulation. These models use a ratio for sigma: laser spot size: diameter of 1:3:10. This was previously determined in paper Johansson, I.E. et al (2014).<sup>2</sup>

Figure 2 depicts the heat of sublimation of H<sub>2</sub>O<sub>(s)</sub>, which is used to determine the value of vaporization while the laser is ablating. Because space is vacuous, H<sub>2</sub>O<sub>(l)</sub> does not appear and H<sub>2</sub>O<sub>(s)</sub> sublimates at sufficient flux levels.

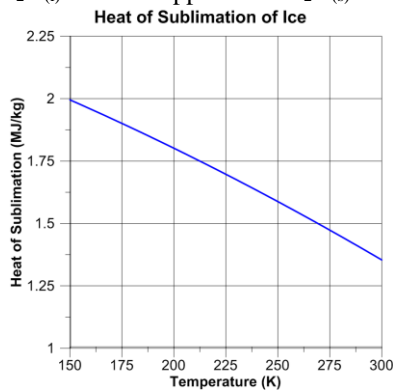


**Figure 2. Heat of Sublimation vs Temperature for H<sub>2</sub>O<sub>(s)</sub>.** This graph depicts the analytically obtained value of sublimation that is used in the subsequent computational models.

## 4. THERMAL ANALYSIS MODELS IN COMSOL

### 4.1. 4D Analytical Model

Using conservation of energy, flux of the laser should be equal to the sum of the flux radiated by the comet, flux conducted into the comet and the flux of the mass ejected. The laser flux is given by a Gaussian beam profile, the flux radiated is given by the Stefan-Boltzmann law, the flux conducted is given by Fourier's law, and the ejected flux is given by Antoine's equation and a modified Langmuir equation.

$$F_{laser} = F_{rad} + F_{cond} + F_{ejecta} \quad (4.1.1)$$

Given laser power  $P$  [W], beam radius  $r$  [m], and the beam's standard deviation  $\chi$  [m], the incoming laser flux is  $F_{laser}$  [ $\text{W m}^{-2}$ ]:

$$F_{laser} = \frac{P}{2\pi\chi} e^{-\frac{r^2}{2\chi^2}} \quad (4.1.2)$$

Given Stefan Boltzmann's constant  $\sigma$  [ $\text{W m}^{-2} \text{K}^{-4}$ ] and the temperature  $T$  [K], the radiation flux is,  $F_{rad}$  [ $\text{W m}^{-2}$ ]:

$$F_{rad} = \sigma T^4 \quad (4.1.3)$$

Given the thermal conductivity  $k$  [ $\text{W m}^{-2} \text{K}^{-1}$ ] and the temperature  $T$  [K], the thermal conduction is  $F_{cond}$  [ $\text{W m}^{-2}$ ]:

$$F_{cond} = k|\nabla T| \quad (4.1.4)$$

The last flux is the most intricate and requires Antoine's equation for pressure. Given the Antoine coefficients  $A$ ,  $B$ , and  $C$  [mmHg] and the temperature,  $T$  [ $^{\circ}\text{C}$ ] the pressure is  $P_V$  [mmHg]:

$$P_V = 10^{A - \frac{B}{T+C}} \quad (4.1.5)$$

Given the coefficient of evaporation  $\alpha_e$ , pressure  $P_V$  [Pa], molar mass  $M$  [ $\text{kg mol}^{-1}$ ], ideal gas constant  $R$  [ $\text{J K}^{-1} \text{mol}^{-1}$ ], and the temperature  $T$  [K], the mass ejection flux is  $\Gamma_e$  [ $\text{kg m}^{-2} \text{s}^{-1}$ ].

$$\Gamma_e = I_e m = \alpha_e P_V \sqrt{\frac{M}{2\pi R_{gas} T}} \quad (4.1.6)$$

Given, the heat of vaporization  $H_{vap}$  [ $\text{J kg}^{-1}$ ], the mass ejection flux  $\Gamma_e$  [ $\text{kg m}^{-2} \text{s}^{-1}$ ], and some handy conversion factors ( $1 \text{ [mmHg]} = 133.32 \text{ [Pa]}$  and  $T \text{ [}^{\circ}\text{C]} = T \text{ [K]} - 273.15$ ), the ejecta flux is  $F_{ejecta}$  [ $\text{W m}^{-2}$ ]:

$$F_{ejecta} = 133.32 H_{vap} \alpha_e 10^{A - \frac{B}{C+T-273.15}} \sqrt{\frac{M}{2\pi R_{gas} T}} \quad (4.1.7)$$

From these definitions of the four fluxes, Comsol solves for the temperatures across the surface and interior of the comet, generating a 4D analytical model. A coordinate system is defined such that the laser beam lies on the x-axis and points in the x direction, while the comet rotates counterclockwise (from x to y) about the z-axis. Equation 4.1.5

provides the vapor pressure. From the vapor pressure and radius  $R$  [m] of a spherical comet, the reaction force,  $\vec{F}_T$  [N], or net thrust, of the ejected plume cloud can finally be calculated:<sup>2</sup>

$$\vec{F}_T = \left\{ -\iint \frac{P_V x}{R}, \quad -\iint \frac{P_V y}{R}, \quad -\iint \frac{P_V z}{R} \right\} \quad (4.1.8)$$

This calculation was done for spherical comets and is therefore an ideal approximation.

### 4.2. Computational Results

The composition of a comet's surface consists mostly of  $\text{H}_2\text{O}_{(s)}$  and volatile ices. As the comet approaches its perihelion (closest to sun in orbit) rapid mass loss occurs on the surface facing the sun due to the YORP effect. This results in fluctuations in its rotation period and solar orbit.<sup>7</sup> Because every comet is unique in size, rotation, and solar orbit, simulations were run of various DE-STAR laser powers, ablating comets of various diameters and rotation periods as seen in Fig. 3 for a 50 m comet. In order to ablate  $\text{H}_2\text{O}_{(s)}$  of a comet with a 50 m diameter, the flux values were kept in the range of  $100 \text{ kW m}^{-2}$  to  $10 \text{ MW m}^{-2}$ , while the object rotated beneath the directed energy beam. During exposure to the directed energy beam the comet's temperature drops, vaporization decreases, causing both a phase shift and magnitude decrease in the average thrust vector. Figure 3 shows the normalized thrust vs time per  $\sigma$ . Each case has many variables that must be taken into consideration. These larger diameters cause the laser beam's energy to disperse across the surface of the comet, leading to a less concentrated laser spot, lower maximum temperature, and, consequently, less thrust.

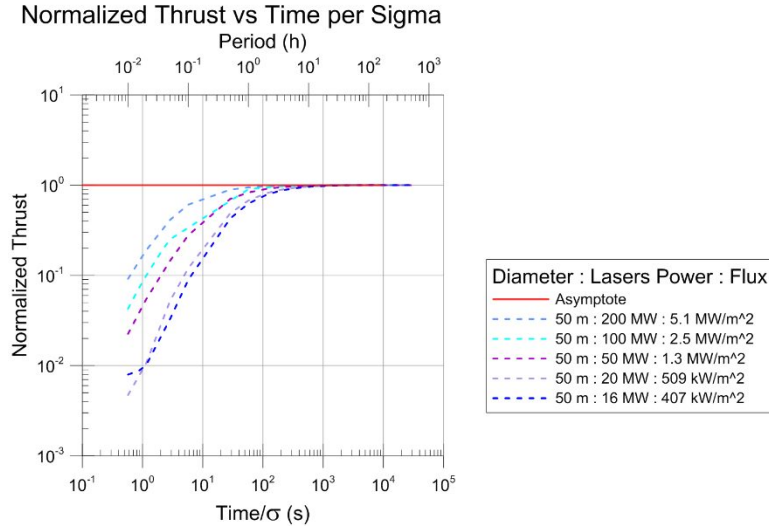
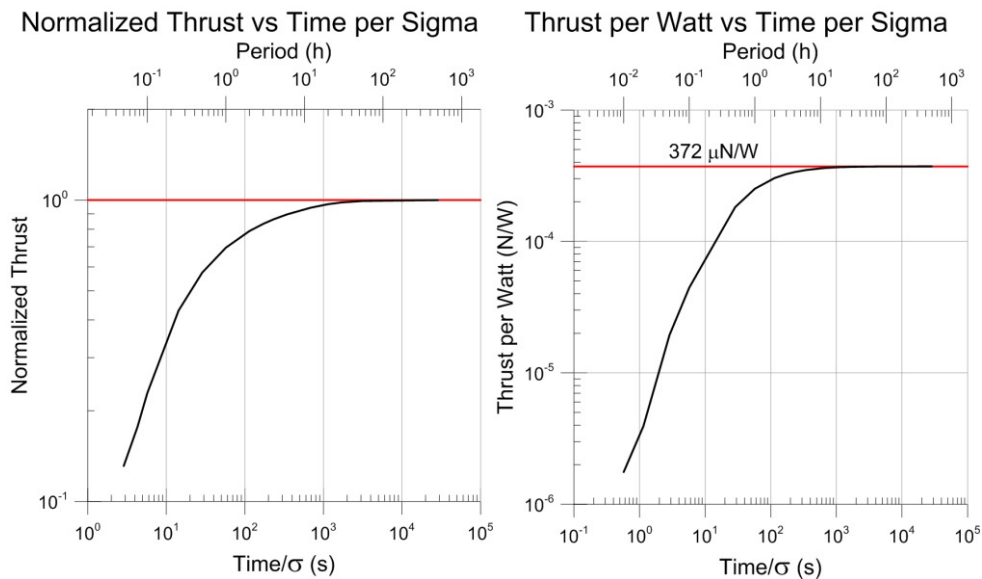


**Figure 3. Normalized Thrust vs Time per  $\sigma$  for various cases.** The larger diameters cause the laser beam's energy to disperse across the surface of the comet, leading to a less concentrated laser spot, lower maximum temperature, and, consequently, lower net thrust.

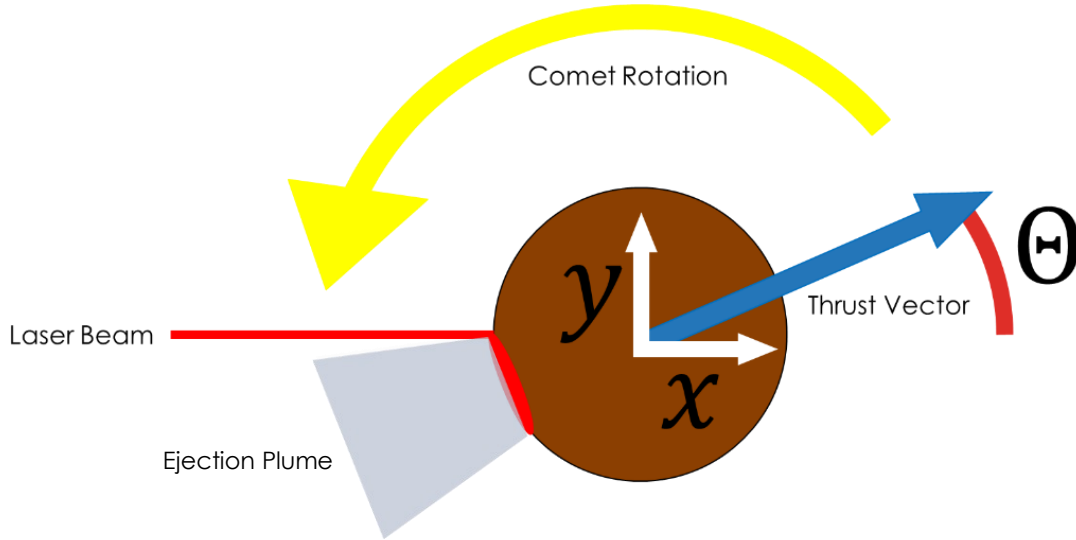
By taking a surface integral of the vapor pressure, the thrust projected onto the comet from the plume of vaporization was calculated. The thrust for each simulation was then normalized and compared, showing a uniform trend. After the comet's temperature has reached equilibrium, the thrust vector's coordinates were then evaluated to determine the trajectory of the comet as it is being ablated, vaporized, and pushed into a new orbit. The coordinates are a valuable resource in evaluating and predicting the comet's new orbit and future destination, hopefully far away from Earth.

Figure 4 and 5 show that, as the time per  $\sigma$  [s] is increased, both the thrust normalized [N] and the thrust per watt [ $\text{N W}^{-1}$ ] increase rapidly until approximately 100 seconds. Then, as the time per  $\sigma$  rises further (comets with slower rotation periods about their axes), the thrust begins to level out to its maximum. This tends to occur within the first couple revolutions once the comet is exposed to the laser, though mass ejection and vaporization, occurs within the first second of exposure to the laser, with a sufficient flux level. Fig. 5 shows the same trend, but with a max thrust per watt of  $\sim 3.72 \times 10^{-4} \text{ N W}^{-1}$ .



**Figures 4. and 5. Thrust per Watt and normalized thrust relative to maximum thrust vs time per  $\sigma$  for the same case as Fig. 3 (50 m diameter  $\text{H}_2\text{O}_{(s)}$  comet, a laser power of 20 MW and a  $\sigma$  of 2.5 m.)**

From rotational mechanics, as a comet's angular velocity increases, its rotation period decreases. Given that the y direction is perpendicular to both the laser direction (x) and the comet's axis of rotation (z), the phase angle, shown in Fig. 6 and 7, is defined here to be the inverse sine of the y-component of thrust divided by the net thrust. With a decrease in rotation period, simulations show that the phase angle approaches a horizontal asymptote of  $\pi/2$  radians.



**Figure 6.** The phase angle is defined in Fig. 6, plotted in Fig. 7, and described in detail later; it is defined as the supplement of the angle between the incoming laser beam and the resultant thrust vector.

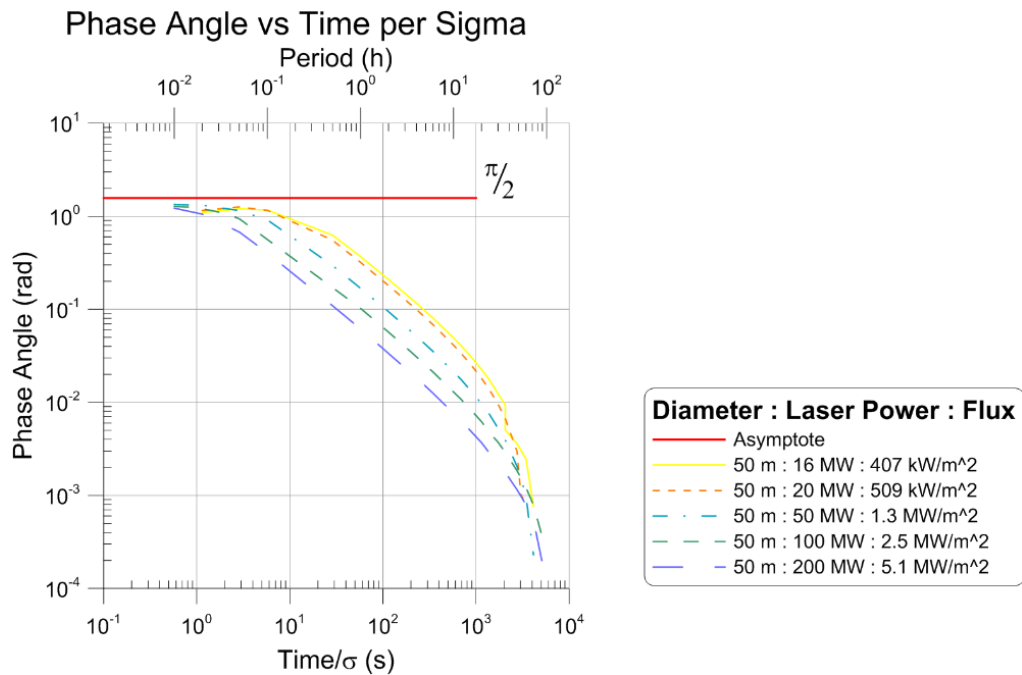


**Figure 7.** Phase angle vs period and time per  $\sigma$  for the case of  $H_2O(s)$ , the phase angle is defined in Fig. 6. With a decrease in rotation period, simulations show that the phase angle approaches a horizontal asymptote of  $\pi/2$  radians. Comparing Fig. 3 to Fig. 7, all the cases increase rapidly in Fig. 3 until about 1 second, while in Fig. 7 the phase angle decreases at the same rate as the thrust in Fig. 3 is increasing. Lastly, notice that the thrust and phase angles are extremely sensitive to temperature. This is all for the same case as Fig. 3, 4, and 5 (50 m diameter  $H_2O(s)$  comet, a laser power of 20 MW and a  $\sigma$  of 2.5 m.)

Given various comet compositions, laser powers, and fluxes, Fig. 8 shows the general trends that the maximum temperatures follow. From these figures, the conclusion can be drawn that temperature and flux are significant factors in computing the net thrust for the ablation of a comet.

Max Temp vs Time per Sigma

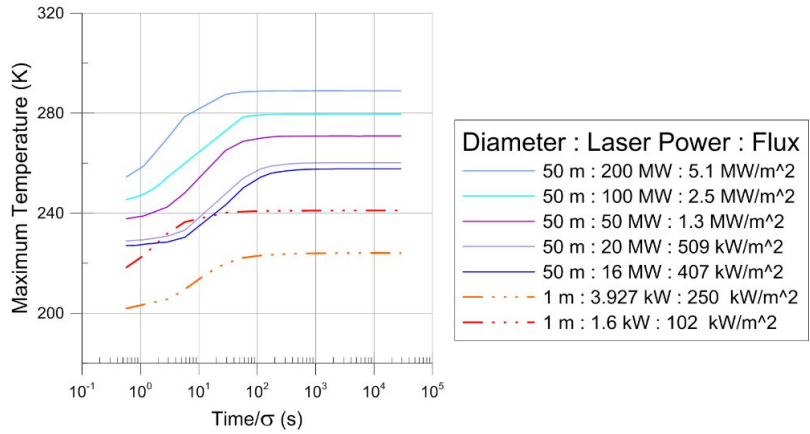


**Figure 8. Maximum temperature vs period and time per  $\sigma$  for all cases.** This is the general trends that the maximum temperatures followed for various cases. When compared to the trend of the thrust and the fluxes observed a correlation can be seen and the conclusion that the temperature and flux are significant factors in computing ablation.

Calculations are performed in the reference frame of the comet. The coordinate system is defined such that the laser beam lies on the x-axis and points in the x direction, while the comet rotates counterclockwise (from x to y) about the z-axis. In Fig. 9, as the rotation period increases (slower rotations), the thrust vector is dominated by its x-component, while the thrust components in both the y and z both approach 0. At short time per  $\sigma$ , the y component decreases, as there is insufficient time to generate strong mass ejection, while at large times, the y component is small due to cooling. There is a maximum y component thrust around a few seconds per  $\sigma$ . The z component is always small, since the comet rotates in the x-y plane.

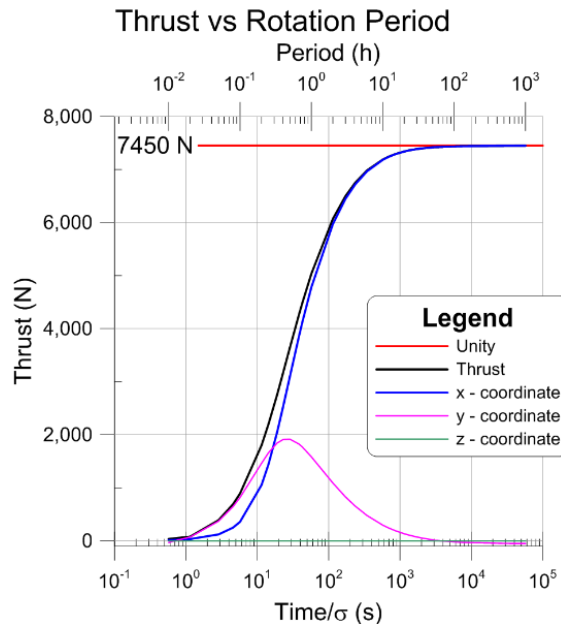


**Figure 9.** This figure shares the same parameters as Figures 2m 3 (laser power of 20 MW,  $\sigma$  of 2.5 m, 50 m diameter). It plots the x, y, and z components and magnitude of the normalized thrust as well as the overall thrust against the rotation period. From this graph you can see that the majority of the thrust is in the x direction and the comet is in the x-y plane, because z coordinate remains close to zero.

As comet rotates, the laser spot ablates a portion of the comet, which revolves away from the spot and begins cooling. While it cools, high surface temperatures and flux levels indicate that this portion of the comet is still being ablated. Thus, the surface continues to induce a vapor pressure and a thrust even when it is not beneath the laser spot. This then adds a component to the thrust vector that is not in the direction of the laser. This can be observed in Fig. 9, where the y-component of thrust is nonzero. At the lower left-hand portion of the graph, the comet is rotating so quickly that the hot spot generated by the laser smears equally across the its surface, generating an equal thrust in all directions and no net force; for a 50 m comet and a  $\sigma$  of 2.5 m, this occurs around one time per  $\sigma$ , which, given those parameter, is equivalent to a period of  $\sim 0.02$  hours or 1.2 minutes.

This result means that greater comet angular velocities will increase the y-component of the thrust vector. This conclusion will have a significant impact on comet steering (direction and manipulation) at high angular velocities. As seen in Fig. 3, the trend is continuous, across various cases.

## 5. CONCLUSIONS

Directed energy is a feasible mechanism for diverting the trajectories of asteroids and comets that threaten to impact Earth. With sufficient flux, surface material on the comet will evaporate, creating a reactionary force as the ejected material leaves the comets. Comets commonly rotate with respect to their orbital frames, and rotation will affect the manner in which a directed energy beam deflects the asteroid or comet. A multi-physics model of a rotating comet has been formulated, based on physical principles of the thrust generated by evaporation of surface material. Many simulations have been performed to characterize the effects of rotation on thrust. Reasonable rotation rates will have only modest effects on deflection, while very rapid rotators will have a large effect on deflection potential. It is also possible to de-spin an asteroid or comet, thus increasing the potential to deflect its orbit and provide valuable aid for future capture or comet mining efforts. Finally, because comet ablation can occur at much lower fluxes than asteroid ablation, from a thermodynamic standpoint, comets will be easier to manipulate than asteroids.

## ACKNOWLEDGMENTS

We gratefully acknowledge funding from NASA NIAC NNX15AL91G and NASA NIAC NNX16AL32G and the NASA California Space Grant NASA NNX10AT93H as well as a generous gift from the Emmett and Gladys W. fund in support of this research.

## REFERENCES

- [1] Lubin, P., Hughes, G. B., Bible, J., Bublitz, J., Arriola, J., Motta, C., Suen, J., Johansson, I. E., Riley, J., Sarvian, N., Clayton-Warwick, D., Wu, J., Milich, A., Oleson, M., Pryor, M., Krogen, P., Kangas, M., and O'Neill, H. "Toward Directed Energy Planetary Defense," *Optical Engineering*, Vol. 53, No. 2, pp 025103-1 to 025103-18 (Feb 2014), doi: 10.1117/1.OE.53.2.025103.
- [2] Johansson, I.E., Tsareva T., Griswold, J., Lubin, P., Hughes, G.B., O'Neill, H., Meinhold, P., Suen, J., Zhang, Q., Riley, J., Melis, C., Walsh, K., Brashears, T., Bollag, J., Mathew, S., and Bible, J. "Effects of asteroid rotation on directed energy deflection," *Proc. SPIE 9226, Nanophotonics and Macrophotonics for Space Environments VIII*, 92607 (September 17, 2014) doi:10.1117/12.2061368
- [3] Riley, J., Lubin, P., Hughes, G. B., O'Neill, H., Meinhold, P., Suen, J., Bible, J., Johansson, I., Griswold, J. and Cook, B. "Directed energy active illumination for near-Earth object detection," Conditionally Accepted for publication by *Journal of Astronomical Telescopes, Instruments and Systems* (Oct, 2014).
- [4] Kosmo, K., Pryor, M., Lubin, P., Hughes, G.B., O'Neill, H., Meinhold, P., Suen, J., Riley, J., Griswold, J., Cook, B.V., Johansson, I.E., Zhang, Q., Walsh, K.J., Melis, C., Kangas, M., Bible, J., Motta, C., Brashears, T., Mathew, S. and Bollag, J. "DE-STARLITE - a practical planetary defense mission," *Nanophotonics and Macrophotonics for Space Environments VIII*, edited by Edward W. Taylor, David A. Cardimona, Proc. of SPIE Vol. 9226, pp. 922604 (Aug, 2014).
- [5] Bottke Jr, William F et al. "The Yarkovsky and YORP effects: Implications for asteroid dynamics." *Annu. Rev. Earth Planet. Sci.* 34 (2006): 157-191.
- [6] Griswold, J., Madajian, J. A., Johansson, I., Pfau, K., Lubin, P., Hughes, G. B., Gilkes, A., Meinhold, P., Motta, C., Brashears, T., and Zhang, Q. "Simulations of directed energy thrust on rotating asteroids," *Nanophotonics and Macrophotonics for Space Environments IX*, edited by Edward W. Taylery, David A. Cardimona, Proc. Of SPIE Vol. 9616, pp. 961606 (2015).

- [7] Squires, R. E. and Beard, D. B. "Physical and Orbital Behavior of Comets." *Astrophysical Journal*, Vol. 133, p. 657 (Mar, 1961).
- [8] Feistel, R. and W. Wagner (2007). Sublimation pressure and sublimation enthalpy of H<sub>2</sub>O ice Ih between 0 K and 273.16 K. *Geochim. cosmochim. acta* 71: 36-45.
- [9] Yaws, C. L. (2007). *The Yaws handbook of vapor pressure: Antoine coefficients*. Houston, Tex: Gulf Pub.
- [10] Gehrels, T., (ed.), *Hazards Due to Comets and Asteroids*, U. of Arizona Press, 1995, pp. 540–543